FULL PAPER

ADVANCED
ENERGY
MATERIALS

Lithium Metal Anodes

www.advenergymat.de

Synergistic Effect of 3D Current Collectors and ALD Surface Modification for High Coulombic Efficiency Lithium Metal Anodes

Kuan-Hung Chen, Adrian J. Sanchez, Eric Kazyak, Andrew L. Davis, and Neil P. Dasgupta*

Improving the performance of Li metal anodes is a critical bottleneck to enable next-generation battery systems beyond Li-ion. However, stability issues originating from undesirable electrode/electrolyte interactions and Li dendrite formation have impaired long-term cycling of Li metal anodes. Herein, a bottom-up fabrication process is demonstrated for a current collector for Li metal electrodeposition and dissolution composed of highly uniform vertically aligned Cu pillars. By rationally controlling geometric parameters of the 3D current collector architecture, including pillar diameter, spacing, and length, the morphology of Li plating/stripping upon cycling can be controlled and optimal cycling performance can be achieved. In addition, it is demonstrated that deposition of an ultrathin layer of ZnO by atomic layer deposition on the current collector surface can facilitate the initial Li nucleation, which dictates the morphology and reversibility of subsequent cycling. This core–shell pillar architecture allows for the effects of geometry and surface chemistry to be decoupled and individually controlled to optimize the electrode performance in a synergistic manner. Using this platform, Li metal anodes are demonstrated with Coulombic efficiency up to 99.5%, providing a pathway toward high-efficiency and long-cycle life Li metal batteries with reduced excess Li loading.

1. Introduction

One of the most attractive strategies to improve energy density and capacity of rechargeable batteries is to replace the graphite anodes currently used in Li-ion batteries (LIBs) with a Li metal anode. Li metal has been widely regarded as an ideal anode material because of its highly negative electrochemical potential and high theoretical specific capacity (3860 mAh g^{-1}), which is a factor of 10 greater than graphite (372 mAh g^{-1}). Moreover,

rechargeable Li metal anodes are a key component required to enable next-generation battery systems including Li–S and Li–air batteries.[1] However, stability issues originating from undesirable electrode/electrolyte interactions and Li dendrite formation have prevented long-term cycling of Li metal anodes. As a result, the performance of Li metal batteries suffer from low Coulombic efficiency (CE), instability against electrolyte decomposition, and formation of 3D topographies including mossy Li, dead Li, and dendrites.[2,3]

Current collectors play a critical role in determining the performance of Li metal batteries because their geometry and surface chemistry both influence the uniformity of Li plating/stripping during cycling. Planar Cu foils have been widely used as a current collector/substrate for Li metal anodes owing to their relatively good stability against Li metal and compatibility with roll-to-roll manufacturing. However, cycling under practical current densities leads to nonuniform Li deposition due to an inhomogeneous Li-ion flux along the electrode surface, resulting in the onset of mossy or dendritic Li growth.[2] The formation of high-surface area Li causes a significant reduction in Coulombic efficiency and eventual cell failure due to undesirable side reactions with the electrolyte as well as "dead" Li formation that results from electrical and/or electrochemical isolation of active Li from the electrode surface.[4] One consequence of these issues has been the need to incorporate excess Li predeposited onto the anode current collector to compensate for losses that occur over the life of the cell. This compromises energy density and complicates manufacturing. In addition to decreasing the cell capacity, uncontrolled Li growth can also cause potential safety hazards as a result of gas evolution and formation of internal short circuits. Therefore, suppressing the formation of high-surface area Li structures during cycling is essential to improve the overall cycle life and efficiency of Li metal batteries.

Recently, there has been a dramatic increase in the number of publications exploring the use of 3D current collectors to address these problems.[5–13] Several studies have shown that by using micro- or nanostructured current collectors, the effective current density can be reduced due to an increase in electroactive surface area, promoting more uniform Li plating/stripping during

K.-H. Chen
Department of Materials Science and Engineering
University of Michigan
Ann Arbor, MI 48109, USA
A. J. Sanchez, E. Kazyak, A. L. Davis, Prof. N. P. Dasgupta
Department of Mechanical Engineering
University of Michigan
Ann Arbor, MI 48109, USA
E-mail: ndasgupt@umich.edu

The ORCID identification number(s) for the author(s) of this article can be found under https://doi.org/10.1002/aenm.201802534.

cell cycling.[3,6,7] In addition, 3D structures can better accommodate the large volumetric changes that occur during Li plating/stripping, which reduces overall cell volume changes. While these studies have demonstrated the advantages of 3D current collectors, they often compare a planar control electrode to a disordered 3D structure,[10–12] rather than rationally controlling geometric parameters in highly ordered structures to achieve an optimal performance. Furthermore, while disordered structures lead to significant increases in surface area, they also introduce significant tortuosity to the electrode, which can lead to mass transport limitations during Li plating/stripping at high current densities. Also, the majority of these works do not explore surface modifications of 3D current collectors to further tune the interfacial chemistry for improved performance. While a few studies have included surface coatings,[8,9] there is a general lack of mechanistic insight into the decoupled roles of geometry and surface chemistry in coated 3D architectures.

In this work, we first demonstrate a bottom-up fabrication process using templated electrodeposition of vertically aligned Cu pillars as a current collector/substrate for Li metal electrodeposition and dissolution. Using the highly ordered arrays of uniform pillars as a model platform, the morphology of Li plating/stripping upon cycling can be controlled by tuning the pillar diameter, pore spacing, and pillar length. Another advantage of the vertical pillar geometry is that tortuosity is reduced to ≈1, as opposed to highly tortuous disordered geometries. In addition, deposition of an ultrathin layer of ZnO by atomic layer deposition (ALD) on the current collector surface is shown to further facilitate uniform Li nucleation, which influences the morphology and reversibility of subsequent Li plating/stripping. The resulting core–shell pillar architecture allows for the geometry and surface chemistry to be decoupled and individually controlled to optimize the electrode performance. Leveraging the synergistic effects of the optimized geometry and interface modification, we have demonstrated cycling of Li metal anodes with Coulombic efficiency of 99.5% at a current density of 0.5 mA cm^{-2} and depth of discharge of 2 mAh cm^{-2} and 99.4% at 1 mA cm^{-2} and 2 mAh cm^{-2}, which are among the highest reported values to date.[14,15]

2. Results and Discussion

2.1. Fabrication and Characterization of Cu Pillar Arrays

Vertically aligned Cu pillar arrays were fabricated using templated electrodeposition, which has been previously used to synthesize metal nanostructures.[16,17] In this approach, a porous polycarbonate track-etched (PCTE) membrane is used as a template and the Cu is electrochemically deposited into the cylindrical pores with well-defined pore sizes (**Figure 1**a).

Unlike randomly textured synthesis methods, templated electrodeposition allows for facile tuning of pillar diameter, spacing, and length across length scales from 50 nm to 50 µm. This allows for rational design of current collector geometry, which can be used to identify tradeoffs between pore volume and spacing, electroactive surface area, electric field localization, and other geometric parameters, all of which affect Li metal morphology. In addition, the templated electrodeposition process can be applied over large areas, while at the same time maintaining high-throughput and cost-effective manufacturing. The compatibility with battery-grade thin Cu foil (18 µm) is also demonstrated here, which suggests that this process can be adapted to large-scale battery manufacturing.

Although potentiostatic conditions are commonly used in templated electrodeposition, Cu pillar arrays plated under constant potential resulted in a relatively large dispersion in the pillar length (Figure S1a, Supporting Information). This has been previously attributed to diffusion limitations into the pores, making it difficult to control the local ion concentration.[18] Such a variation in pillar length is not favorable, as it may introduce spatial inhomogeneities in the electrochemical
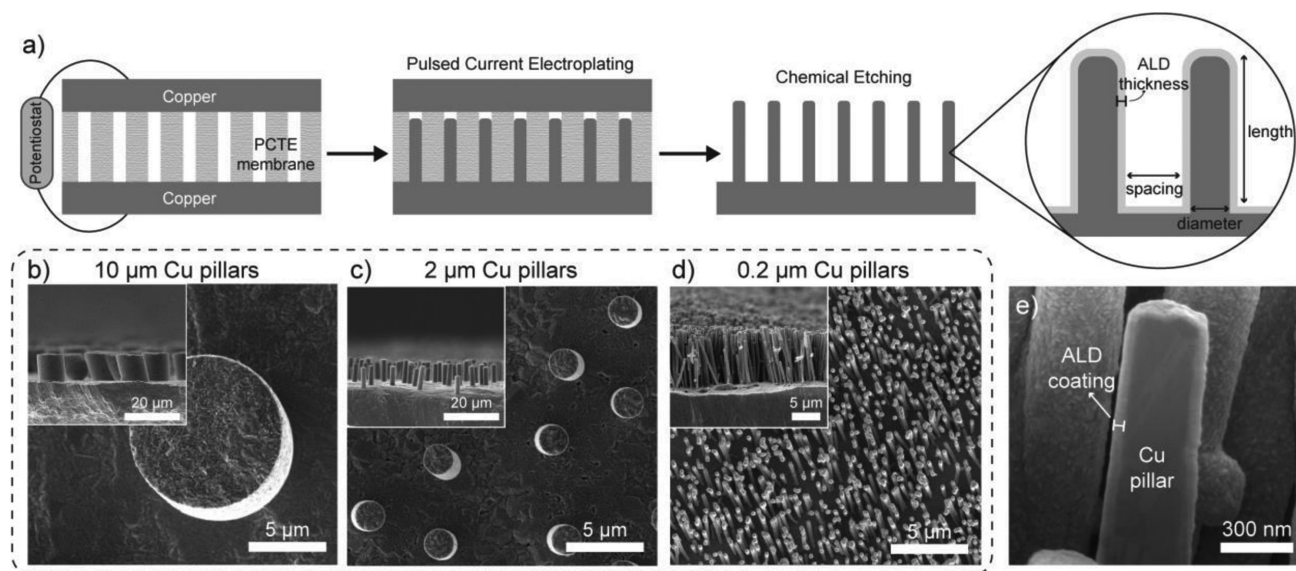

Figure 1. a) Schematic illustration of the templated electrodeposition process of the Cu pillar arrays. Top-down and cross-section SEM images of the b) 10 µm, c) 2 µm, and d) 0.2 µm Cu pillars. e) Cross-section focused ion beam (FIB)-SEM image of the core-shell ALD-coated Cu pillar structure.

**ADVANCED
SCIENCE NEWS**
www.advancedsciencenews.com

**ADVANCED
ENERGY
MATERIALS**
www.advenergymat.de

performance of Li plating/stripping, especially near the current collector–separator interface. To avoid this geometric variation, pulsed current electrodeposition was adopted instead, in which the current was periodically interrupted to relax concentration gradients during the plating process.[18] By carefully tuning electrodeposition parameters, Cu pillar arrays with highly uniform length can be achieved (Figure S1b, Supporting Information).

Additional geometric parameters, including pillar diameter and pore spacing, can be rationally controlled through selection of the appropriate template (Figure 1a). The pillar length is determined by the membrane thickness and/or the electroplating time duration. To demonstrate the tunable design of Cu pillar arrays as current collectors, PCTE membranes with pore diameters of 10, 2, and 0.2 µm were used in this work. The surface porosity (open area) of all membranes was fixed at 8% ± 2% and the resulting Cu pillar length was initially controlled to be 10 ± 0.5 µm. Figure 1b–d shows the scanning electron microscopy (SEM) images of 10, 2, and 0.2 µm Cu pillar arrays, respectively. The cross-sectional SEM images indicate the good vertical alignment of the Cu pillars on the planar Cu foil. Grazing incidence X-ray diffraction (GIXRD) analysis verified that the Cu pillars were crystalline without any traces of impurities (Figure S2, Supporting Information).

2.2. Morphology Analysis upon Li Plating and Stripping

To investigate the behavior of Li plating/stripping on planar and 3D Cu current collectors, Li–Cu cells were assembled and cycled galvanostatically at a current density of 1 mA cm^{-2}. 1 M LiTFSI in 1:1 DOL:DME (1,3-Dioxolane : 1,2-Dimethoxyethane) with 1 wt% LiNO$_3$ was used as the electrolyte. Cu pillars with diameters of 0.2, 2, and 10 µm were systematically studied. Since both the surface porosity of the membrane (8%) and pillar length (10 µm) were fixed, the available open volume for Li deposition was essentially identical for all three geometries, allowing for up to 2 mAh cm^{-2} to be deposited within the open volume. Owing to the constant surface porosity, the average spacing between each pillar was fixed at ≈2.5 times larger than the given pillar diameter (e.g., 2 µm pillar arrays have an average pore spacing of 5 µm; further details in the Supporting Information).

Figure 2a–c shows the morphology of Li plating/stripping on a planar Cu electrode at various points in the cycle. After 0.5 mAh cm^{-2} of Li deposition, spherical Li deposits with varying sizes were observed on the planar Cu surface with a nonuniform surface coverage (Figure 2a). This morphology is often attributed to an inhomogeneous Li-ion flux along the planar Cu surface. After 1 mAh cm^{-2} of Li plating, the Li deposits branched out as elongated and needle-like dendrites (Figure 2b). After Li stripping, a large amount of "dead Li" and solid electrolyte interphase (SEI) residue were found to remain on the electrode surface (Figure 2c), which can be attributed to the incomplete dissolution of dendrite structures, leading to their detachment and electrochemical isolation from the electrode surface.[4]

In contrast, a drastically different Li morphology was observed on the 2 µm Cu pillar arrays (Figure 2g–i). Spherical Li deposits with identical size and uniform coverage over the

whole electrode surface were observed upon 0.5 mAh cm^{-2} of Li plating (Figure 2g). The improved Li morphology can be attributed to the reduced local current density and more homogeneous Li-ion flux within the 3D structure, which promoted uniform plating. Cross-sectional SEM analysis shows that the Li deposits filled into the void space between Cu pillars and deposited conformally along the side walls of the Cu pillars (Figure S3, Supporting Information). Interestingly, these agglomerated deposits were confined to grow laterally within the pillar arrays rather than outward toward the counter electrode, which is another unique feature of the vertical pillar geometry. This is attributed to penetration of the top surface of the pillars into the separator, as discussed in detail below. After 1 mAh cm^{-2} of Li plating, Li spheres agglomerated and merged together as compact Li deposits (Figure 2h) with morphologies significantly different than the needle-like dendrites observed on planar Cu. As a result of a more compact morphology, less dead Li was observed after Li stripping (Figure 2i), exposing the clean Cu pillar surface. This reduction in dead Li indicates that the 2 µm Cu diameter pillar arrays can improve the reversibility of cycling.

To test the effect of further reducing the pillar diameter and spacing on Li deposition, 0.2 µm diameter Cu pillar arrays (with an average pore spacing of 0.5 µm) were used as a current collector. As shown in Figure 2d, Li deposits appear to grow on top of the pillar arrays rather than within the 3D structure. Cross-sectional SEM analysis (Figure S4, Supporting Information) confirmed that the deposits were almost exclusively formed on top of the pillars. After 1 mAh cm^{-2} of Li plating, Li deposits continued to grow into larger spheres (Figure 2e). Three possible mechanisms can simultaneously contribute to this phenomenon, described below.

First, the 0.2 µm pillar sample has an increase in electrode surface area by a factor of 10x compared to the 2 µm pillar geometry. This will reduce the local current density along the Cu pillar surface. It has been previously proposed that continually increasing surface area can promote an improved morphology. However, in the case of a planar Cu current collector, it has also been shown that decreasing current density favors more sparse nucleation and growth of larger diameter Li deposits to a lower driving force for nucleation at low current densities.[19] Therefore, since the pore spacing between the 0.2 µm pillar diameter arrays (0.5 µm) is well below the observed diameter of the plated Li deposits (>1 µm),[19] this indicates that growth of initial nuclei on the top surface is favored compared to that of nuclei confined within the void space between pillars (Supporting Information). This also illustrates the value of rational design of a 3D current collector architecture, as increasing surface area and decreasing pore spacing can lead to competing effects.

Second, the 0.2 µm Cu pillars have an aspect ratio of 50, which can cause significant current focusing at the tips of the pillars, further promoting preferential nucleation at the top of the array. Third, the narrow and long void space can introduce diffusion limitations during plating. As the Li-ion concentration depletes toward the bottom of the pores, local Li deposition is suppressed.

As a consequence of both of these additional effects, the local current density at the tips is higher than along the sidewalls. Both of these two additional factors will couple with the first
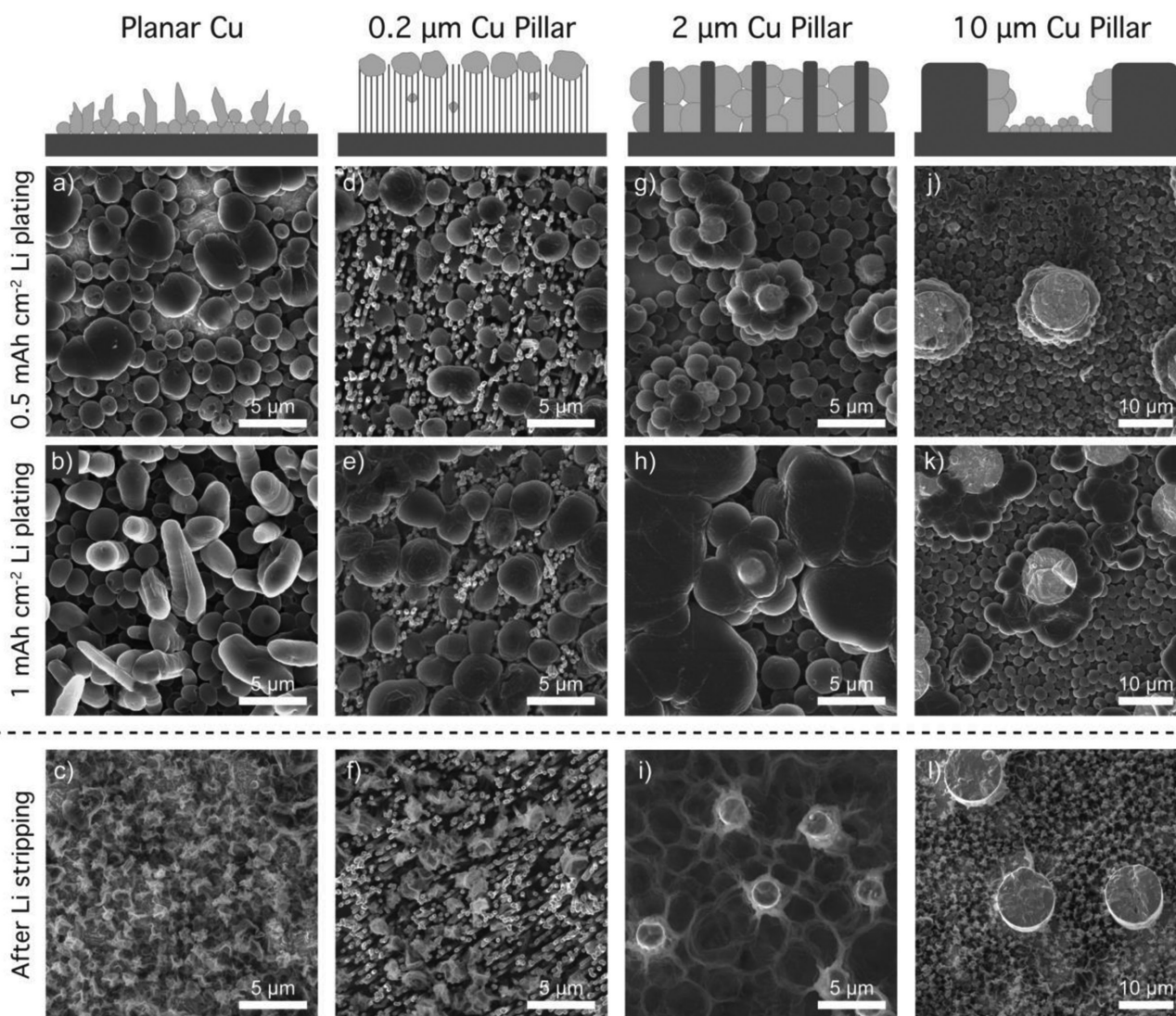
Figure 2. Schematics and SEM images of Li deposition and dissolution on the Cu current collectors. a–c) planar Cu electrode, d–f) 0.2 µm Cu pillars, g–i) 2 µm Cu pillars, and j–l) 10 µm Cu pillars upon 0.5 mAh cm^{-2} of Li plating, 1 mAh cm^{-2} of Li plating, and after Li stripping, respectively. The current density was fixed at 1 mA cm^{-2}.

mechanism and further exacerbate the Li deposition on the top surface instead of within the 3D structure. Combining these three mechanisms, we can conclude that

1) Nucleation density is a function of local current density.
2) Larger deposits that would normally grow at lower current densities are constrained by the small pore diameter, suppressing their growth.
3) Owing to the high aspect-ratio of the 0.2 µm pillars, the local current density is higher at the top of the electrode, thus enhanced nucleation and growth.

After stripping the Li deposited on the top surface of the 0.2 µm pillars, significantly more dead Li was observed, compared to the 2 µm geometry (Figure 2f). This illustrates the importance of optimizing the nucleation kinetics along the

entire active surface of a 3D current collector to facilitate reversible plating within the 3D geometry. Furthermore, since these surface and volume effects are both dependent on geometry, this also motivates the ability to decouple surface kinetics from the geometric architecture, which will be demonstrated later in this paper through the use of ALD surface modification.

To study the impact of increasing pillar diameter and pore spacing, Li plating was also tested on Cu pillars with a 10 µm diameter and an average pore spacing of 25 µm. Upon 0.5 mAh cm^{-2} of Li plating, spherical Li deposits appear to uniformly cover the entire electrode surface (Figure 2j). As the deposition proceeded (1 mAh cm^{-2}), Li deposits agglomerated around the Cu pillars (Figure 2k). However, owing to the wide pore spacing between Cu pillars, Li deposition failed to merge into a compact layer. In particular, a significant fraction of Li plated on the bottom surface of the electrode, resembling

the morphology of the planar electrode. After stripping, a large amount of dead Li was still observed, along the bottom surface (Figure 2l). This suggests that with increasing pore spacing, a significant fraction of the current collector surface resembles a planar electrode. It is therefore important to engineer the pillar spacing and electrode surface area to facilitate merging of larger Li deposits within the pore volume.

This knowledge gained from the highly ordered model system of vertical pillars provides valuable insight into the rational design of 3D current collectors, which may also take alternate geometric form factors. For example, in this study, the total pore volume was maintained as a constant, allowing us to focus on the impact of varying electrode geometry for a fixed total volumetric capacity of the electrode. However, further optimization based on these observed trends can be applied to alternate geometries, depending on the battery application desired.

The 3D Cu pillar architecture also displayed favorable mechanical properties for battery manufacturing, as it did not plastically deform in the assembly and/or disassembly of a coin cell, as shown in the SEM images (Figure 2). To confirm these observations, a finite element model was developed in ABAQUS (Supporting Information) which showed that only small strains ($\approx 10^{-4}$) would occur in the Cu pillars subject to compression within the cell, which are safely within the elastic limits of Cu. Therefore, the Cu pillar arrays do not sustain any permanent deformation, which make them viable for battery manufacturing.

Another significant and unique benefit of the highly uniform vertical pillar geometry was the observation that despite the potential for strong electric field localization near the top surface of the pillars, no Li deposition occurred on the pillar tips for the 2 and 10 µm diameter samples (Figure 2g–l). Instead, the Li deposition on the pillar surfaces occurred exclusively along their sidewalls (Figure S3, Supporting Information).

A potential explanation for this phenomenon is that the separator is mechanically deformed when sandwiched against the Cu pillars, effectively masking off the top portion of the pillars from electrolyte. The strain analysis from the ABAQUS model provides support for this suggestion, where highly localized compressive strains ($\approx 10^{-1}$) can develop in the polymer separators as they deform around the pillar tips, which will likely reduce their local porosity. This reduction in local porosity can in turn limit the exposure of electrolyte to the top surface of the pillars and reduce the local ionic flux at the pillar tips during cycling. As the current will follow the path of least resistance, this would promote growth along the pillar sidewalls, which are not in contact with the separator, as shown in the finite element model. To further support this hypothesis, a cell was assembled without a separator using the 2 µm diameter geometry. The SEM analysis shows that without the presence of the separator, Li deposition occurs uniformly along the Cu pillar surface, including the tops of the pillars (Figure S5, Supporting Information), demonstrating the role of local compressive contact with the separator on protecting the tips.

The suppression of growth at the pillar tops is highly beneficial from a safety standpoint, as it reduces the probability of a catastrophic internal short circuit, which could otherwise be amplified by electric field focusing at vertical protrusions on a nonplanar surface. Even if dendritic structures were to

form, the growth of lateral structures within the pores would appear to drive them more toward compressive stress against nearest neighbor pillar sidewalls, leading to a more compact morphology as observed in the 2 µm diameter samples. In contrast, in highly disordered 3D current collectors, including vertical pillars with nonuniform heights, this benefit would not be expected to play as significant of a role.

2.3. Electrochemical Performance of Cu Pillar Arrays

To evaluate the cycling performance of the Cu pillar arrays, Li–Cu cells were assembled and characterized by their CE. A convenient method that is often used to determine the Coulombic efficiency is to use exhaustive Li stripping for each cycle. In that approach, a given amount of Li is initially plated onto the Cu electrode (Q_P), followed by a stripping half cycle that ends when a cutoff voltage is reached (Q_S). This cutoff indicates that all the removable Li has been stripped from the Cu surface.[20] While this method can provide a cycle-by-cycle efficiency (CE = 100% $\times Q_S/Q_P$), the Li loss associated with side reactions between Li and Cu electrode cannot be avoided during Li deposition process. As a result, the measured CE is convoluted and highly dependent of the current collector material and surface conditions. Moreover, this method is not reflective of practical Li metal batteries since these typically incorporate excess Li.

A more representative method of determining Li CE was proposed and systematically investigated by Adams et al.[20] In this method, the Cu electrode is first preconditioned with a single Li plating/stripping cycle, which leads to formation of a passivation layer that stabilizes the surface against further reaction with the Cu surface. Next, a Li reservoir (Q_T) is deposited, which is followed by n stripping/plating cycles with a fixed capacity of Li less than the initial Li reservoir ($Q_C < Q_T$). The remaining Li on the Cu electrode is then completely stripped to a cutoff voltage (Q_S). Using this protocol, an average value of CE can be determined using the following equation: $CE_{avg} = 100\% \times (nQ_C + Q_S)/(nQ_C + Q_T)$.[20] This method is more accurate since the initial surface passivation cycle reduces effects from initial side reactions between Li and Cu, and it better reflects practical Li metal battery designs, in which a limited amount of excess Li is always present to account for Li loss during cycling.[21]

Using the method described above, the electrochemical performance of planar Cu and 3D current collectors were compared. Specifically, the Cu electrodes were first conditioned by plating 2 mAh cm^{-2} of Li and then stripping the deposit until a cutoff voltage of 0.5 V was reached. A Li reservoir of 2 mAh cm^{-2} (Q_T) was then deposited on the Cu electrodes, followed by cycling for either 10 or 20 cycles with a depth of discharge of 1 mAh cm^{-2} (Q_C). The Li was then fully stripped from the Cu until the voltage reached the cutoff of 0.5 V to determine Q_S and the average CE (Figure S6, Supporting Information). In addition, long-term cycling was carried out to quantify the cycling lifetime. It is noted that a fixed current density (e.g., 1 ± 0.005 mA cm^{-2}) was applied throughout the cycling to ensure a consistent CE measurement.

Figure 3a shows the galvanostatic cycling of Li–Cu cells with 0.2, 2, and 10 µm Cu pillar arrays at a current density of 1 mA cm^{-2}. The cells were cycled until cell failure occurred,
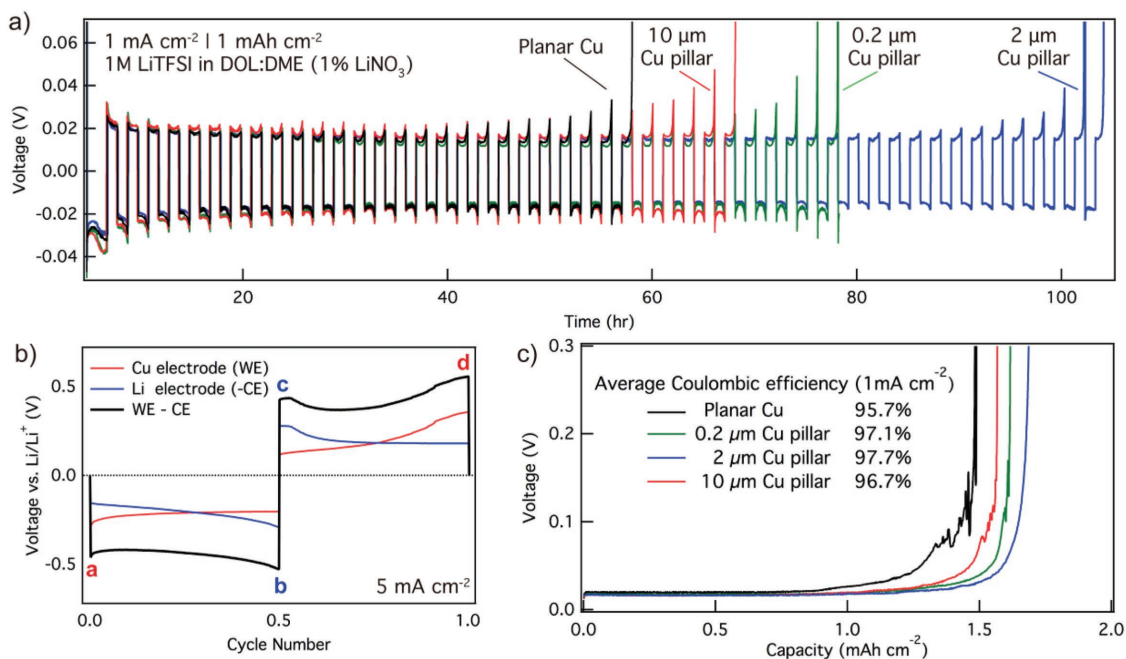
ADVANCED
SCIENCE NEWS

www.advancedsciencenews.com

ADVANCED
ENERGY
MATERIALS

www.advenergymat.de

Figure 3. a) Galvanostatic cycling of Li–Cu cells at 1 mA cm^{-2} for 1 mAh cm^{-2} on the planar Cu and Cu pillars of 0.2 μm, 2 μm, and 10 μm diameters. A Li reservoir of 2 mAh cm^{-2} was first deposited onto the Cu electrodes before cycling. b) Three-electrode measurements showing the cell polarization contributions from the Cu working electrode (WE) and Li counter electrode (CE). CE voltage has been inverted for visual clarity. c) Voltage profile of the last Li dissolution from Cu showing remaining capacity after ten cycles of Li stripping/plating. The average Coulombic efficiency for each configuration is provided in the inset as an indicator of the loss of reversible Li.

which is signified by a sharp increase in cell polarization. The 3D current collectors all displayed an improved cycle life when compared to the planar Cu sample. However, the best performance was exhibited by the 2 μm Cu pillar arrays that had a cycle life of >100 h (50 cycles). This is almost double the cycle life of the planar specimen (60 h; 28 cycles).

To better understand the observed voltage variations during cell cycling and the failure mechanism, three-electrode measurements were performed to decouple the voltage contributions from Li and Cu electrode. Figure 3b shows the overall voltage profile of a full cycle (black) and the decoupled voltage traces from the Cu working electrode (WE, red) and Li counter electrode (blue). It is clear that the initial peak in the first half cycle (peak a) can be attributed to Li nucleation overpotential on the Cu electrode, whereas the peak toward the end of the second half cycle (peak d) was associated with stripping Li from Cu.[22]

Since the Li reservoir on the Cu current collector was continuously consumed during cycling as a result of the imperfect CE, the amount of available Li was gradually depleted at later cycles. A sharp increase in overpotential (trend in peak d in Figure 3a) was observed as a result of Li depletion on the Cu current collector, which was defined as the failure point to determine cycle lifetime. Similarly, as Li depletion on the Cu electrode progresses with each cycle, new Li deposits in the subsequent plating cycle must nucleate on the Cu surface to a greater and greater extent rather than grow on any residual Li. Consequently, a higher nucleation overpotential (peak a) was also observed as complete depletion of the plated Li is approached and the experiment is terminated. On the other hand, peak b and c can be attributed to the Li electrodissolution

(peak b) and deposition (peak c) on the Li metal counter electrode.[22] Because an effectively "infinite" amount of excess Li was present, Li plating/stripping on the Li metal electrode exhibited a very stable cell polarization throughout the cycling (Figure 3a).

The three-electrode measurements confirm that the failure mode is due to Li depletion on the Cu current collector as a result of the continuous Li consumption during Li plating/stripping process. The poor performance of the planar Cu is therefore attributed to an undesirable Li deposition morphology causing excessive SEI and dead Li formation, which results in early depletion of the Li reservoir. On the other hand, the improved cycle life of the 2 μm Cu pillar arrays can be explained by the growth of agglomerated and compact Li deposits, which minimizes the formation of SEI and dead Li during cycling.

This analysis also suggests that cell failure is not convoluted by other failure modes. For example, it has been shown that both dead Li accumulation and electrolyte consumption (leading to a dry cell) can contribute to eventual cell failure when using an exhaustive Li stripping cycling protocol,[24] which can convolute the real performance of the Cu electrode. These phenomena can be decoupled in the cycling method described above. To further demonstrate the accuracy of this approach, a cell with significantly smaller volume of electrolyte was assembled and cycled. Despite the reduced electrolyte volume, cell failure was not affected, indicating that Li depletion on the Cu electrode still occurred sooner the depletion of electrolyte (Figure S7, Supporting Information).

To quantify the average CE of the current collectors, a full strip after 10 and 20 cycles was performed respectively (Figure 3c
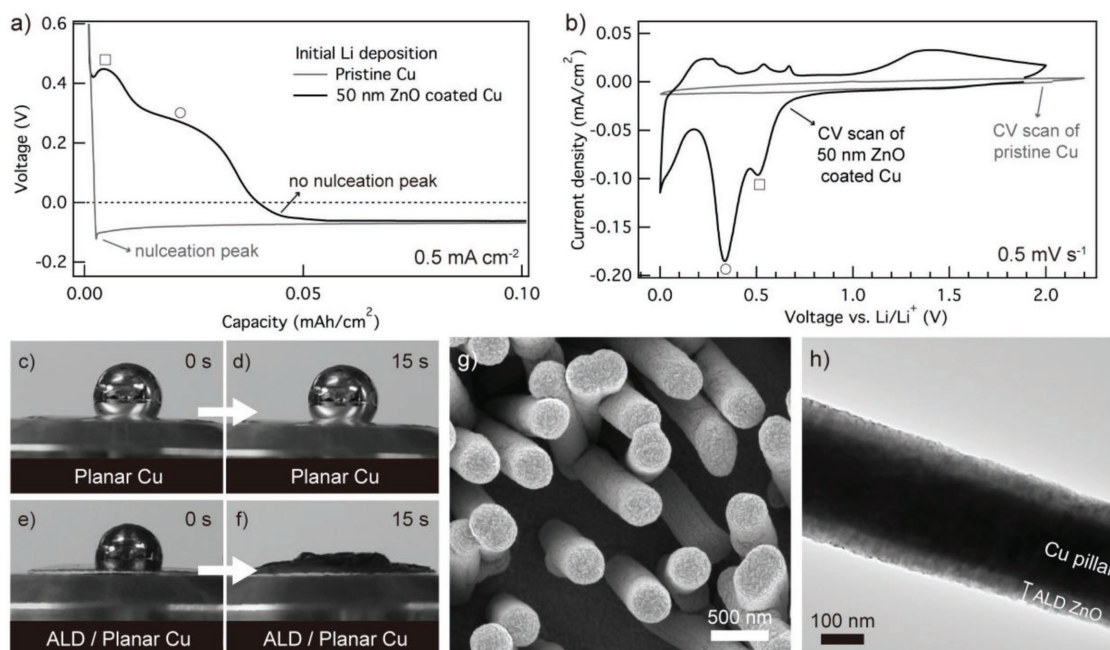
ADVANCED
SCIENCE NEWS
www.advancedsciencenews.com

ADVANCED
ENERGY
MATERIALS
www.advenergymat.de

Figure 4. a) Voltage profiles of the pristine and ALD ZnO coated planar Cu during initial Li deposition at 0.5 mA cm^{-2}. b) CV scans of the pristine and ALD ZnO coated planar Cu at a scan rate of 0.5 mV s^{-1}. c,d) Contact angle measurements of molten metallic Li on pristine planar Cu showing the poor Li wettability of pristine Cu surface over time. e,f) Contact angle measurements on ALD ZnO coated planar Cu. g) SEM image of ALD-coated Cu pillars showing nanocrystalline ZnO grains. h) TEM image showing the conformal ZnO coating (50 nm) on the 200 nm Cu pillar.

and Figure S8, Supporting Information). The efficiency values for a given geometry exhibited a very small variation regardless of the cycle number, which verified the precision of this cycling protocol. Under a current density of 1 mA cm^{-2}, the average CEs were: 95.7% for the planar Cu current collector; 96.7% for the 10 µm pillars, and 97.7% for the 2 µm Cu pillars and 97.1% for the 0.2 µm Cu pillars (Figure 3c).

The morphological and electrochemical analysis above demonstrate the impact of the rational design of 3D current collector structures. By controlling geometric parameters, the Li morphology upon plating/stripping can be greatly modulated, which significantly affects the cycling efficiency and lifetime. It is shown that vertically aligned Cu pillar arrays with adequate pore spacing (≈5 µm) to accommodate the Li deposits exhibited improved performance compared to current collectors with either greater or smaller pillar spacing as well as the planar Cu current collector. The need for rational design in an ordered model system rather than using random and disordered structures as current collector is thus warranted. This also indicates a very important point that while several works have demonstrated enhanced performance of porous nanostructures, the geometries may not comprise the optimal dimensions.

2.4. Tuning Interfacial Chemistry by ALD Surface Modification

While the above analysis shows that using Cu pillar arrays as a current collector can boost the cycling efficiency and lifetime, there still exists a large nucleation peak during the initial Li deposition, indicating a substantial nucleation barrier (**Figure** 4a). This barrier represents the thermodynamic cost of forming

critical Li nuclei, which is governed by the interfacial energy between the Cu current collector and Li metal. A recent study by Yan et al. reported that while some materials exhibit large nucleation overpotential upon Li deposition (Cu, Ni, C, etc.), others show a nucleation overpotential of nearly zero (Au, Ag, Zn, etc.).[23] The absence of a nucleation overpotential has been attributed to the reactions of "lithiophilic" materials with Li metal to form a buffer layer consisting of alloys and solid solution phases at the interphase of the substrate and the pure Li phase, which can eliminate nucleation barriers upon Li deposition.

In this work, we further apply this concept to modify the surface of the Cu pillar arrays to tune the interfacial chemistry. It is worth noting that while a few reports have previously explored surface modification of 3D current collectors,[8,24–27] the role of geometry and surface chemistry in 3D geometries has not been systematically decoupled and studied. This is partially due to the difficulty of applying a conformal coating over the porous microstructure surfaces in a controllable manner while preserving the 3D structure. In order to address this issue, we used ALD to deposit a conformal coating on the surface of the Cu pillar arrays. ALD is a thin film deposition technique comprised of gas-phase surface reactions that are cyclically repeated to build up a uniform, conformal, and pinhole-free thin film.[28,29] Owing to its vapor phase precursors and self-limiting chemistry, ALD can deposit highly conformal thin films on high-aspect-ratio substrates with sub-nanometer thickness control. In addition, many ALD thin films can be deposited at low temperatures and in an inert environment, which also opens opportunities for coating on battery active materials.[30] Recent progress has demonstrated using ALD to deposit thin protection layers directly on Li metal anode surfaces can improve the cycling

ADVANCED
SCIENCE NEWS
www.advancedsciencenews.com

ADVANCED
ENERGY
MATERIALS
www.advenergymat.de

performance.[31–33] However, to date, a systematic study of the CE of Li electrodeposition on ALD-modified planar and 3D current collector architectures with rationally controlled geometric parameters is lacking, which is necessary to decouple the roles of geometry, surface chemistry, and wettability on Li plating morphology and reversibility.

Here, ZnO is chosen as the coating material because the electrochemical reaction of ZnO upon lithiation results in the formation of Li_xZn alloy, which can serve as the buffer layer for the subsequent Li deposition. Previous research efforts have shown that the lithiation reactions of ZnO can be described as a two-step process involving a conversion reaction followed by alloying:[34–36]

$$ZnO + 2Li \leftrightarrow Zn + Li_2O \qquad (1)$$

$$Zn + xLi \leftrightarrow Li_xZn \, (x \leq 1) \qquad (2)$$

To test the electrochemical stability of the ALD ZnO, a thin layer of 50 nm ZnO was first deposited onto a planar Cu electrode. Cyclic voltammetry (CV) measurements were then performed in a potential window of 0–2 V (vs Li/Li+). Figure 4b shows the CV curve of the first scan. The initial cathodic sweep of the CV exhibited two characteristic peaks at 0.5 and 0.33 V, which represent the conversion reaction where the ZnO is reduced by Li to form elemental Zn and Li_2O and the alloying reaction between Li and Zn.[37] Similarly, during the anodic sweep, the multistep dealloying process of the Li_xZn alloy was represented by peaks between 0.25 and 0.65 V, whereas the peak centered at 1.4 V has been associated with the reformation of ZnO.[37,38] To further verify the effect of the ALD ZnO coating, a CV measurement was also performed using a pristine Cu electrode. As shown in Figure 4b, no characteristic peak was observed throughout the CV scan, suggesting no electrochemical reaction occurred on the pristine Cu surface.

Figure 4a further shows the voltage profile of ALD ZnO coated Cu electrode upon Li deposition under a current density of 0.5 mA cm−2. Two characteristic plateaus are present in the voltage profile, which match the peaks observed in the CV cathodic scan. Upon further Li deposition, a smooth voltage trace was observed, without the presence of the nucleation peak that occurred on the pristine Cu (Figure 4a). This suggests that the Li nucleation overpotential on ALD ZnO is essentially zero. Therefore, even an ultrathin layer (50 nm) of ZnO on the Cu current collector can significantly change the interfacial chemistry. The formation of Li_xZn alloy during lithiation reactions of ALD ZnO can serve as a "buffer layer" to facilitate the subsequent Li nucleation and deposition on top of the ZnO surface once it is fully lithiated. X-ray photoelectron spectroscopy analysis and open-circuit voltage measurements were also performed to show that the plated Li formed on top of the buffer layer, without the presence of measurable Zn on the Li surface (Figures S9 and S10, Supporting Information). Therefore, we show that the mechanism of the ZnO buffer layer is to facilitate an initially homogeneous Li flux into the ALD film, followed by subsequent Li plating on the fully lithiated ZnO surface.

Recent studies have also demonstrated that the coupling between surface chemistry and Li wettability can directly impact the electrochemical performance of Li metal batteries.[39,40] To quantitatively measure the lithiophilicity of ALD ZnO coated Cu, molten Li contact angle measurements were performed using a sessile drop test of pure Li without the presence of native surface layers.[39] As shown in Figure 4c,d, the molten Li droplet exhibited a large contact angle on the pristine Cu surface that remained constant over time, indicating the poor wettability between Li and Cu (Video S1, Supporting Information). In contrast, Li droplet exhibited a smaller initial contact angle on the ALD ZnO coated Cu surface, and quickly spread out over the entire surface (Figure 4e–f and Video S2, Supporting Information). The time-dependent morphology of the molten Li also illustrates the importance of reporting video data using a sessile drop test, rather than a single photograph in time, which may not represent the full evolution of the wetted state. The drastic difference in the wetting process can be attributed to the conversion and alloying reactions between Li and ZnO, leading to improved Li wettability.

To demonstrate the capability of ALD to deposit conformal films on the 3D pillar geometry, 50 nm ZnO was deposited on the 0.2 µm arrays. As shown in Figure 4g, a conformal ZnO thin film with nanocrystalline grains from the as-deposited ZnO can be clearly observed. More importantly, the ALD coating perfectly preserves the pillar architecture, which allows for the geometry and surface chemistry to be decoupled and individually controlled to optimize the electrochemical performance. Transmission electron microscopy (TEM) analysis further confirmed the uniform thickness and core–shell geometry of the ALD film on the pillar surface (Figure 4h). XRD measurements verified the polycrystallinity of the as-deposited ZnO film on Cu pillar arrays (Figure S11, Supporting Information).

2.5. ALD Surface-Modified Cu Pillar Arrays during Li Plating/Stripping

To investigate the behavior of Li plating/stripping on ALD ZnO coated current collectors, Li–Cu cells were cycled galvanostatically at a current density of 1 mA cm−2. A dramatically different Li morphology is observed when the planar current collector is coated with ALD ZnO (**Figure 5**a–c). Upon 0.5 mAh cm−2 of Li plating, significantly larger Li deposits are formed on the electrode and packed in a more compact manner (Figure 5a). Further deposition (1 mAh cm−2) leads to compact and agglomerated Li spheres without any trace of dendritic structures (Figure 5b). After Li stripping, a much "cleaner" electrode surface is revealed, indicating improved cycling reversibility and less dead Li formation. These results suggest that an ultrathin thin layer of ZnO can effectively facilitate the initial Li nucleation, producing morphologies better suited for cycling.

Figure 5d–f further shows the synergistic effect of ALD coating on the 2 µm Cu pillars during cycling. Larger Li deposits are again observed during Li deposition and also confined to grow within the void space between pillars, without coating the pillar tops (Figure 5d,e). After stripping, significantly less dead Li remained on the electrode surface (Figure 5f) than in the uncoated pillars (Figure 2i). It is also
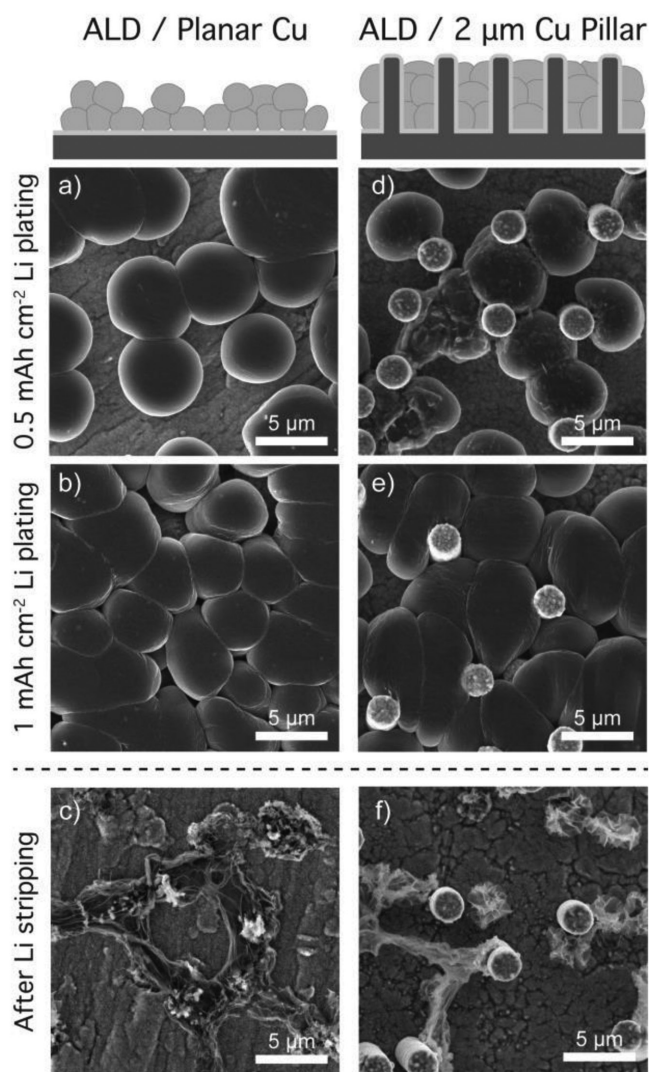
**ADVANCED
SCIENCE NEWS**
www.advancedsciencenews.com

**ADVANCED
ENERGY
MATERIALS**
www.advenergymat.de

Figure 5. SEM analysis of a–c) ALD-coated planar Cu and d–f) ALD-coated 2 µm Cu pillars upon 0.5 mAh cm^{-2} Li plating, 1 mAh cm^{-2} Li plating, and after Li stripping. The current density was fixed at 1 mA cm^{-2}.

noted that while Li deposition mainly occurred on top of the pristine 0.2 µm Cu pillars, ALD coated 0.2 µm pillars exhibited a dramatically different morphology, where the Li deposits appear to grow within the 3D structure (Figure S12, Supporting Information). This further demonstrates the importance of decoupling electrode geometry and surface chemistry effects on morphology and cycling in order to rationally design 3D current collector architectures.

2.6. Electrochemical Performance of ALD Surface-Modified Cu Pillar Arrays

To demonstrate the synergistic effect of the ALD surface modification and 3D geometry on electrochemical performance, Li–Cu cells with ALD coated planar Cu and 2 µm Cu pillar arrays were assembled and cycled. ZnO films of 10, 20, 50, and

100 nm were first deposited onto a planar Cu electrode and cycled to measure efficiency and cycle life (Figure S13, Supporting Information). Similar cycling lifetimes and average CEs were obtained regardless of the varying ALD thickness. Therefore, 50 nm of ALD ZnO was chosen as the surface modification for further experiments using ALD coated pillar arrays.

Figure 6a shows the voltage profiles of planar Cu, 2 µm pillars, ALD/planar Cu, and ALD/2 µm pillars upon cycling at a current density of 1 mA cm^{-2}. With the ALD ZnO surface treatment on the planar Cu, the cell exhibited stable cycling up to 120 h (59 cycles), doubling the cycle life of pristine planar Cu (60 h; 28 cycles). Furthermore, with the synergistic effect of ALD surface modification and optimized 2 µm pillar array structure, the cycling lifetime can be tripled (>180 h; 91 cycles), as shown in the Figure 6a.

Average CE measurements were also performed over 10 and 20 cycles (Figure 6b and Figure S14, Supporting Information). While the pristine planar Cu exhibited a low CE of 95.7%, an enhancement to 98.1% was observed with the addition of an ALD ZnO surface coating. Moreover, when the ALD ZnO coating was applied to 2 µm pillar arrays, a CE as high as 99.3% was achieved with a current density of 1 mA cm^{-2} and 99.5% at 0.5 mA cm^{-2} (Figure 6b and Figure S15, Supporting Information). It is noted that ALD-coated 0.2 and 10 µm pillar arrays also displayed improved performance compared to uncoated pillars, yet the 2 µm pillar diameter remained the optimal geometry (Figure S16, Supporting Information). The Coulombic efficiency values for both pristine and ALD-coated pillar arrays are further summarized in Figure 6d.

Stable Li plating/stripping with higher per-cycle areal capacity can also be achieved through increasing the length of the Cu pillar arrays (Figure S17–18, Supporting Information). Increasing length, while maintaining the same diameter and spacing of the template allows us to increase the total capacity of the electrode, and therefore cycle a larger volume of Li per cycle. Figure 6e summarizes the average Coulombic efficiency values under varying current densities and areal capacities. As shown, increasing the pillar length (and therefore enabling larger depth of discharge) further increased the CE to 99.4% at 1 and 2 mA cm^{-2} at 2 mAh cm^{-2}. These values are among the highest reported to date (Table S1, Supporting Information), illustrating the benefits of the 3D pillar architecture and ALD surface modification to systematically design optimized electrodes.

The above analysis has demonstrated the synergistic effect of both the 3D current collector geometry and ALD surface modification to achieve high CE Li metal anodes and decouple the mechanistic effects of each. The ALD coated 2 µm Cu pillar arrays not only exhibited a much higher CE of 99.3% compared to planar Cu (95.7%), but it also tripled the cycle life when galvanostatically cycled at 1 mA cm^{-2}. This enhanced electrochemical performance can reduce the amount of required excess Li metal loading in Li metal batteries, thus increasing the overall specific energy and energy density. To demonstrate this, an uncoated, planar Cu electrode with a Li reservoir of 4 mAh cm^{-2} (instead of 2 mAh cm^{-2}) was cycled, as shown in Figure 6c. In order to obtain a similar cycle life to the ALD coated 3D current collector, the required amount of excess Li needs would need to increase by a factor of more than two.
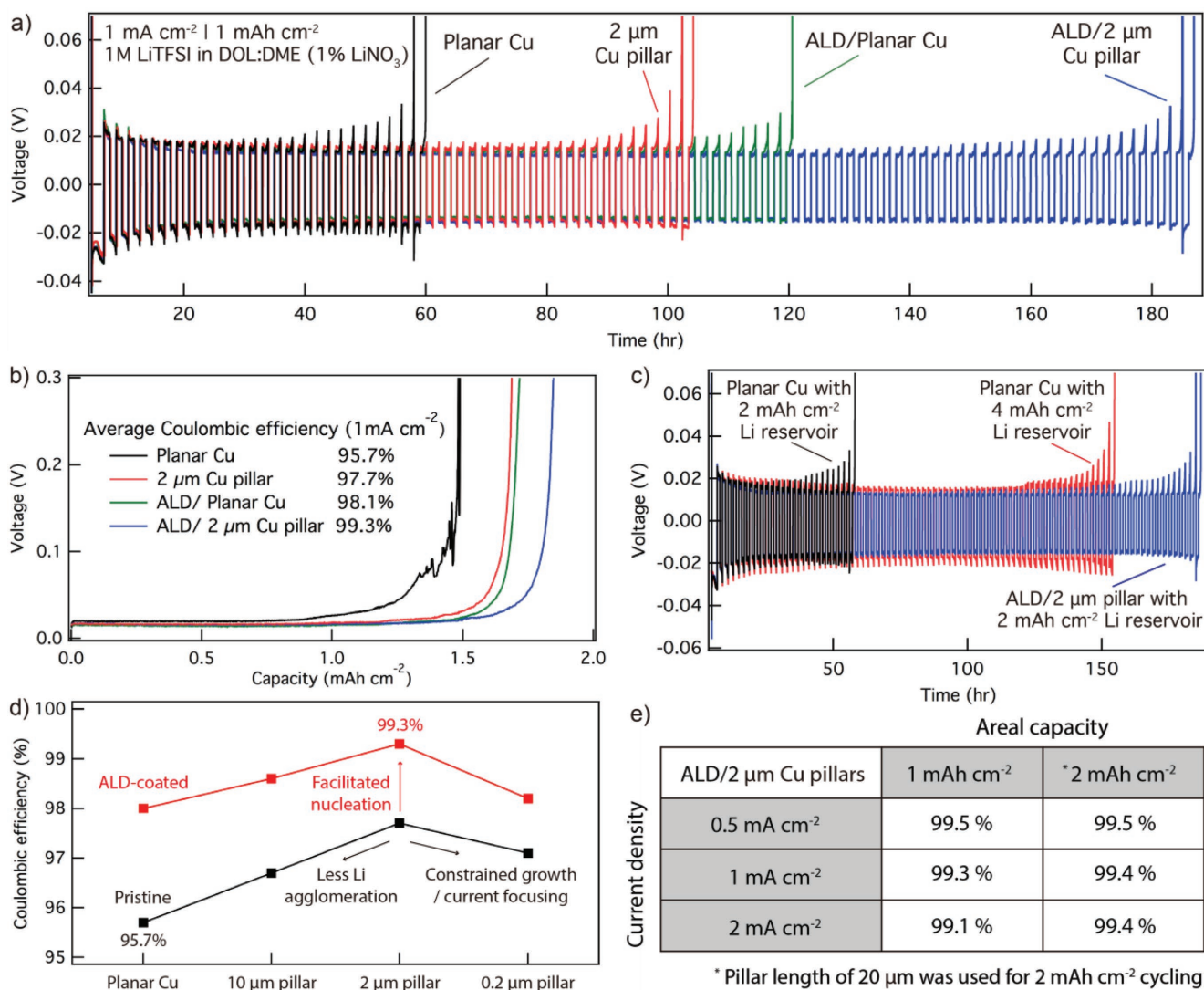
Figure 6. a) Cycling performance of the pristine and ALD-coated planar Cu and 2 µm Cu pillars at 1 mA cm^{-2} for 1 mAh cm^{-2}. b) Average Coulombic efficiency measurements after ten Li stripping/plating cycles. c) Cycling performance of the planar Cu (black) and ALD-coated 2 µm Cu pillars (blue) with a Li reservoir of 2 mAh cm^{-2} and the planar Cu with a Li reservoir of 4 mAh cm^{-2} (red). d) Coulombic efficiency plot for both pristine and ALD-coated pillar arrays at 1 mA cm^{-2} and 1 mAh cm^{-2}. e) Average Coulombic efficiency of ALD-coated 2 µm pillar arrays under varying current densities and areal capacities.

3. Conclusion

In this work, we have demonstrated the fabrication of vertically aligned and highly uniform Cu pillar arrays on a Cu foil via templated electrodeposition for use as a 3D current collector. With this highly ordered model platform, we demonstrated that the rational design of 3D current collector, combined with ALD surface modification, can be used to achieve improved Li plating and stripping morphology and CE. The results in this paper have led to several key points of understanding:

1) The geometry of the 3D current collector has a significant impact on the Li morphology upon Li plating/stripping, which affects the CE and cycle life. This emphasizes the

critical need to rationally control the geometric parameters of 3D current collectors in order to achieve the desired Li morphology. Cu pillar arrays of 2 µm pillar diameter and an average pore spacing of 5 µm exhibited compact and uniform Li deposition and displayed improved performance compared to both larger and smaller diameters and spacing. This can be attributed to a number of factors, including local current density, electric field focusing, ionic diffusion, and separator interactions. These variables in turn affect the nucleation density, average growth size and shape of deposits, and dead Li formation.

2) The vertical pillar architecture can cause local deformation of separators when compressed against the Cu pillars, which appears to block Li-ion flux on the tops of the pillars and causes Li deposition to preferentially occur within the pores

rather than on top of the pillar arrays. This minimizes the risk of hazardous short circuiting of the battery, as Li growth occurs in the void space between the pillars, rather than outward toward the counter electrode. However, if the diameter and spacing of the rods become too small (as in the 0.2 µm sample), this effect is insufficient to overcome the driving force for preferential growth at the top surfaces

3) ALD ZnO surface modification can be further applied to the Cu pillar arrays to tune the interfacial chemistry, which is a powerful technique to deposit highly conformal thin films on high-aspect-ratio Cu pillars with precise thickness control. An ultrathin layer (50 nm) of ALD ZnO appears to facilitate more homogeneous Li nucleation, resulting in larger and more densely packed Li morphologies, as well as more reversible Li plating/stripping. With the synergistic effect of the 3D geometry and surface modification, the ALD coated 2 µm pillar arrays exhibited a high CE up to 99.4% under a current density of 1 mA cm^{-2} and 99.5% under a current density of 0.5 mA cm^{-2}.

4) This study has shed light on several important parameters for designing and manufacturing optimized 3D current collectors. The model system of highly ordered and uniform pillars allows us to decouple input variables that have been previously coupled in the vast majority of studies of 3D current collectors for Li metal anodes. The insights gained from this work can therefore be further applied to rational design of alternate 3D architectures.

Supporting Information

Supporting Information is available from the Wiley Online Library or from the author.

Acknowledgements

Conflict of Interest

The authors declare no conflict of interest.

Keywords

[1] P. G. Bruce, L. J. Hardwick, K. M. Abraham, *MRS Bull.* **2011**, *36*, 506.
[2] K. N. Wood, M. Noked, N. P. Dasgupta, *ACS Energy Lett.* **2017**, *2*, 664.
[3] D. Lin, Y. Liu, A. Pei, Y. Cui, *Nano Res.* **2017**, *2*, 1.
[4] K.-H. Chen, K. N. Wood, E. Kazyak, W. S. LePage, A. L. Davis, A. J. Sanchez, N. P. Dasgupta, *J. Mater. Chem. A* **2017**, *5*, 11671.
[5] L. Kong, H. J. Peng, J. Q. Huang, Q. Zhang, *Nano Res.* **2017**, *10*, 4027.
[6] C.-P. Yang, Y.-X. Yin, S.-F. Zhang, N.-W. Li, Y.-G. Guo, *Nat. Commun.* **2015**, *6*, 8058.
[7] S.-H. Wang, Y.-X. Yin, T.-T. Zuo, W. Dong, J.-Y. Li, J.-L. Shi, C.-H. Zhang, N.-W. Li, C.-J. Li, Y.-G. Guo, *Adv. Mater.* **2017**, *29*, 1703729.
[8] C. Yang, S. Yao, S. He, H. Xie, E. Hitz, L. Hu, *Adv. Mater.* **2017**, *29*, 1.
[9] C. Zhang, W. Lv, G. Zhou, Z. Huang, Y. Zhang, R. Lyu, H. Wu, Q. Yun, F. Kang, Q.-H. Yang, *Adv. Energy Mater.* **2018**, *8*, 1703404.
[10] Q. Yun, Y.-B. He, W. Lv, Y. Zhao, B. Li, F. Kang, Q.-H. Yang, *Adv. Mater.* **2016**, *28*, 6932.
[11] Q. Li, S. Zhu, Y. Lu, *Adv. Funct. Mater.* **2017**, *27*, 1606422.
[12] L.-L. Lu, J. Ge, J.-N. Yang, S.-M. Chen, H.-B. Yao, F. Zhou, S.-H. Yu, *Nano Lett.* **2016**, *16*, 4431.
[13] D. Lin, Y. Liu, Z. Liang, H.-W. W. Lee, J. Sun, H. Wang, K. Yan, J. Xie, Y. Cui, *Nat. Nanotechnol.* **2016**, *11*, 626.
[14] Y. Liu, Y. K. Tzeng, D. Lin, A. Pei, H. Lu, N. A. Melosh, Z. X. Shen, S. Chu, Y. Cui, *Joule* **2018**, *2*, 1.
[15] S. Chen, J. Zheng, D. Mei, K. S. Han, M. H. Engelhard, W. Zhao, W. Xu, J. Liu, J. G. Zhang, *Adv. Mater.* **2018**, *30*, 1706102.
[16] M. T. Barako, S. Roy-Panzer, T. S. English, T. Kodama, M. Asheghi, T. W. Kenny, K. E. Goodson, *ACS Appl. Mater. Interfaces* **2015**, *7*, 19251.
[17] M. Motoyama, Y. Fukunaka, T. Sakka, Y. H. Ogata, S. Kikuchi, *J. Electroanal. Chem.* **2005**, *584*, 84.
[18] P. L. Taberna, S. Mitra, P. Poizot, P. Simon, J.-M. Tarascon, *Nat. Mater.* **2006**, *5*, 567.
[19] A. Pei, G. Zheng, F. Shi, Y. Li, Y. Cui, *Nano Lett.* **2017**, *17*, 1132.
[20] B. D. Adams, J. Zheng, X. Ren, W. Xu, J.-G. Zhang, *Adv. Energy Mater.* **2017**, *8*, 1702097.
[21] P. Albertus, S. Babinec, S. Litzelman, *Nat. Energy* **2018**, *3*, 16.
[22] K. N. Wood, E. Kazyak, A. F. Chadwick, K.-H. Chen, J.-G. Zhang, K. Thornton, N. P. Dasgupta, *ACS Cent. Sci.* **2016**, *2*, 790.
[23] K. Yan, Z. Lu, H.-W. Lee, F. Xiong, P.-C. Hsu, Y. Li, J. Zhao, S. Chu, Y. Cui, *Nat. Energy* **2016**, *1*, 16010.
[24] L. L. Lu, Y. Zhang, Z. Pan, H. Bin Yao, F. Zhou, S. H. Yu, *Energy Storage Mater.* **2017**, *9*, 31.
[25] S. Liu, X. Xia, Y. Zhong, S. Deng, Z. Yao, L. Zhang, X.-B. Cheng, X. Wang, Q. Zhang, J. Tu, *Adv. Energy Mater.* **2017**, *8*, 1702322.
[26] C. Jin, O. Sheng, J. Luo, H. Yuan, C. Fang, W. Zhang, H. Huang, Y. Gan, Y. Xia, C. Liang, J. Zhang, X. Tao, *Nano Energy* **2017**, *37*, 177.
[27] Y. Zhang, W. Luo, C. Wang, Y. Li, C. Chen, J. Song, J. Dai, E. M. Hitz, S. Xu, C. Yang, Y. Wang, L. Hu, *Proc. Natl. Acad. Sci. USA* **2017**, *114*, 3584.
[28] S. M. George, *Chem. Rev.* **2010**, *110*, 111.
[29] N. P. Dasgupta, H.-B.-R. Lee, S. F. Bent, P. S. Weiss, *Chem. Mater.* **2016**, *28*, 1943.
[30] X. Meng, X.-Q. Yang, X. Sun, *Adv. Mater.* **2012**, *24*, 3589.
[31] E. Kazyak, K. N. Wood, N. P. Dasgupta, *Chem. Mater.* **2015**, *27*, 6457.
[32] A. C. Kozen, C. F. Lin, A. J. Pearse, M. A. Schroeder, X. Han, L. Hu, S. B. Lee, G. W. Rubloff, M. Noked, *ACS Nano* **2015**, *9*, 5884.
[33] L. Chen, J. G. Connell, A. Nie, Z. Huang, K. R. Zavadil, K. C. Klavetter, Y. Yuan, S. Sharifi-Asl, R. Shahbazian-Yassar, J. A. Libera, A. U. Mane, J. W. Elam, *J. Mater. Chem. A* **2017**, *5*, 12297.

[34] A. Kushima, X. H. Liu, G. Zhu, Z. L. Wang, J. Y. Huang, J. Li, *Nano Lett.* **2011**, *11*, 4535.

[35] H. Asayesh-Ardakani, W. Yao, Y. Yuan, A. Nie, K. Amine, J. Lu, R. Shahbazian-Yassar, *Small Methods* **2017**, *1*, 1700202.

[36] C. Wang, Y. Gong, B. Liu, K. Fu, Y. Yao, E. Hitz, Y. Li, J. Dai, S. Xu, W. Luo, E. D. Wachsman, L. Hu, *Nano Lett.* **2017**, *17*, 565.

[37] X. Shen, D. Mu, S. Chen, R. Huang, F. Wu, *J. Mater. Chem. A* **2014**, *2*, 4309.

[38] X. H. Huang, X. H. Xia, Y. F. Yuan, F. Zhou, *Electrochim. Acta* **2011**, *56*, 4960.

[39] A. Sharafi, E. Kazyak, A. L. Davis, S. Yu, T. Thompson, D. J. Siegel, N. P. Dasgupta, J. Sakamoto, *Chem. Mater.* **2017**, *29*, 7961.

[40] X. Han, Y. Gong, K. Fu, X. He, G. T. Hitz, J. Dai, A. Pearse, B. Liu, H. Wang, G. Rubloff, Y. Mo, V. Thangadurai, E. D. Wachsman, L. Hu, *Nat. Mater.* **2017**, *16*, 572.